

# ELASTOPLASTIC CONSTITUTIVE LAW FOR CONCRETE EXPOSED TO HIGH TEMPERATURE: CHEMOPLASTIC MODELING

RABAH HAMMOUD\*

\* École Polytechnique de Montréal  
C.P. 6079, Succ. Centre-Ville, Montréal (Québec), Canada H3C 3A7  
e-mail: rabah.hammond@polymtl.ca, www.polymtl.ca

**Key words:** Concrete, High temperature, Constitutive law, Chemoplastic, Elastoplastic material, Failure.

**Abstract:** To adequately simulate the behavior of concrete exposed at high temperature, a new constitutive model was proposed. The particularity of our model is the fact that dehydration is considered as chemoplastic softening. Whereas traditional methods adopt conventional models of elastoplasticity and try to vary certain parameters dependent on local temperature. Under chemoplastic framework, we also proposed a new yield criterion which was experimentally fitted. To realistically reproduce the impact of high temperature on concrete durability under different loading modes, new ductility function was proposed and fitted to a wide range of dehydration processes. The hardening and softening functions are defined in terms of the acting confining pressure. The inelastic dilatancy of concrete is expressed through the non associate flow rule. In this fact, new chemoplastic potential was proposed and fitted to ensure better estimate of the load directions. The prediction capabilities of the model are demonstrated and numerical predictions are compared with experimental results. The comparison reveals that the model accurately predicts different stress states of concrete under different temperature treatments.

## 1 INTRODUCTION

In the last two decades, serious fires in high-rising building and tunnels have been leading to increased research interest in material behaviour under extremely high temperatures. Fire may affect the strength and reduces drastically the load-carrying capacity and, under certain circumstances, the concrete surface could spall due to thermal expansions and the development of high gas pressures in the pores [1].

Under elevated temperature exposure, cement matrix experiences physical and chemical changes that contribute to development of shrinkage, transient creep, and changes in mechanical properties and durability. Key factor affecting the properties of concrete at high temperature are its moisture state (i.e. sealed or unsealed),

chemical structures (i.e. loss of chemically bound water from the *CSH* in the unsealed condition, CaO/SiO<sub>2</sub> ratio of the hydrate in sealed conditions, and amount of Portlandite, [Ca(OH)<sub>2</sub>]), and physical structure, i.e. total pore volume including cracks and average pore size [2,3].

To develop a reliable formulation of concrete, it is essential to understand behavior of concrete both during and after exposure to elevated temperature. It is also necessary to assess effects of thermal degradation in order to develop predictive tools and validate design codes. Degradation of concrete can be evaluated by numerical models. Many structural problems can be adequately simulated by an elastoplastic model. That elastoplastic framework modeling is indeed well adapted to many structural problems, and is mostly used to simulate behavior of concrete

under various load types.

Classical way of taking into account dependence of mechanical behaviour of concrete on temperature is to use conventional models of elastoplasticity and to vary certain parameters [5-7]. The temperature dependence in the existing models has the main effect of changing the strength of materials. Several models are proposed to study the material under fire. Ahmad and Hamoush [4] suggested a nonlinear elastic model for modelling the compression behaviour of concrete at isothermal conditions at high temperatures. This model does not reproduce the increased sensitivity to the confinement of multiaxial compressive strength of concrete.

Nechnech et al. [6] and Luccioni et al. [7] have developed a coupled elastoplastic-damage model for structures subject to thermal stress. They hypothesized that plasticity effects are decoupled from other phenomena. Modelling of material was performed under assumptions of the thermodynamics of irreversible processes. Nechnech et al adopted multi-surface criterion to represent more adequately material response under different triaxial loadings. Multi-surface criterion is seen as a superposition of mechanisms where each mechanism is managed by its own loading surface [8]. The brittle behaviour can be managed by Rankine criterion and the ductile phase (compression) by Drucker-Prager criterion, taking into account the hydrostatic pressure [6].

As part of the analysis of the fire in the Chunnel tunnel, Ulm et al. present a radically different formulation [9]. Indeed, they consider the behaviour of plain concrete subjected to high temperatures as the reverse of the hydration of young concrete. This was treated as a coupled thermo-chemo-mechanical problem [10,11]. During hydration, development of the resistance and stiffness with the degree of hydration is treated as chemo-plastic hardening. Thus, dehydration becomes a chemo-plastic softening. Their model was developed respecting thermodynamics of closed reactive porous media as posed by Coussy [12].

Based on the theory of porous media

developed by Ulm and Coussy [10], Cervera et al [13] present a coupled thermo-chemo-mechanical model considering the effect of aging on the evolution of various mechanical properties of concrete. Hellmich et al [14] have treated the coupling thermo-chemo-mechanical shotcrete. Their model is extended to a chemo-plastic model and uses two failure surfaces: a cut in traction and the surface of Drucker-Prager in compression. The plastic volumetric expansion serves as hardening variable.

We propose a new approach based of chemo-plasticity considering dehydration as chemo-plastic softening of concrete while exposed to high temperature. There is difference between our model and standard models of thermo-plasticity of concrete at high temperatures using criteria that depend on temperature [5-7]. Indeed, using hardening force as a parameter implies that dehydration (not temperature) is partly behind the decrease in strength that is observed macroscopically. Origin of decohesion is considered chemical (not thermal), and can be explained as follows: at microscopic level, dehydration process can be attributed to micro-diffusion of chemically bonded water molecules from the micropores to capillary pores. Loss of bound water, chemical decomposition, and dissociation of hydrated products weaken the chemical structure of cement gel by destroying the cohesive forces in the micro-pores. At macroscopic scale, these phenomena lead to a chemical decohesion affecting the resistance domain and its evolution. It was found that the compressive strength decreases linearly with the degree of dehydration. It follows that the dependence  $f_c = f_c(\xi)$  is intrinsic material function and has a mechanical sense unlike the phenomenological relation  $f_c = f_c(T)$ .

## 2 DEGREE OF DEHYDRATION AS CHEMOELASTIC INDEX

Using the linear chemo-mechanical coupling theory [9,11], the degree of dehydration is defined as follow:

$$\xi = \frac{f_c(T)}{f_c} \quad (1)$$

where  $f_c(T)$  is the uniaxial compressive strength at temperature  $T$ ,  $f_c$  is the uniaxial compressive strength at ambient temperature. As depicted in Figure 1, the variation is proportional clearly linear. Figure 2 shows the evolution of the degree of dehydration as a function of temperature. The degree of dehydration is given calculated by thermoactivated kinetics, which is typically a time-dependent non linear ordinary differential equation (*ODE*). Degree of dehydration significantly decreases after exposure to high temperatures. For example, the degree of dehydration were 100% and 64% when the concrete was at virgin state and heated at 300°C, respectively. It seems that the dehydration process spends on a two stages: before and after 300°C.

On the material level, high temperatures lead to an irreversible loss of elastic stiffness (thermal damage) and of material strength (thermal decohesion) of concrete. Both are generally described by an apparent temperature dependence of the material properties of concrete. Thermal damage is hence expressed as variation of elastic modulus  $E = E(T)$  as a function of temperature, while thermal decohesion is expressed as variation of compressive strength  $f_c = f_c(T)$ . However, thermal damage cannot be explained, at the microscopic level, as a dependency of mechanical properties of concrete on temperature. Indeed, the mechanical properties are related to the concentration and structure of the constituents of the cement paste that change significantly with the dehydration process. On a macroscopic level, this can be translated as a dependency relationship between the elastic properties of the material and the mass of hydrates. Using thermal decohesion as chemoplastic softening means that dehydration (not temperature) has, in part, caused the decrease in strength observed macroscopically.

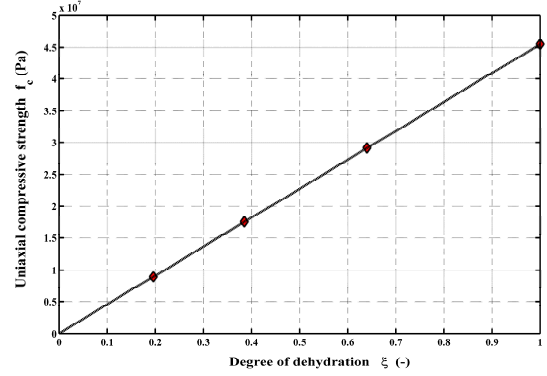


**Figure 1:** Degree of dehydration of the concrete after exposure to elevated temperature

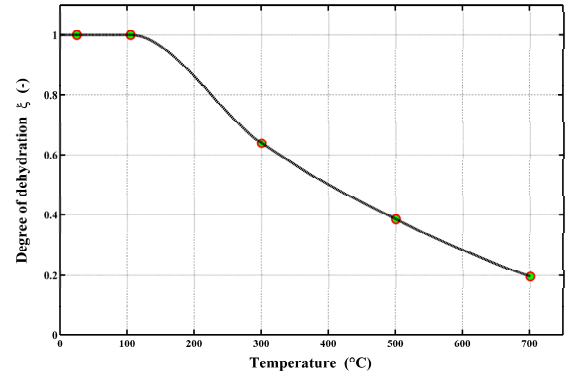


**Figure 2:** Evolution of the degree of dehydration versus temperature exposure

### 3 FORMULATION OF THE CONSTITUTIVE MODEL

#### 3.1 Loading surface

In this study, the triaxial constitutive formulation of concrete at high temperature is based on the extended Leon model (*ELM*). This model features a non-associated flow theory of plasticity with isotropic hardening and isotropic softening in the pre- and post-peak regime, respectively. The encompassing loading surface proposed by Etse and Willam [15] can be used to describe the triaxial behavior of the material in a wide range of loading histories as follow:

$$\begin{aligned}
 & F(\sigma_m, \rho, r(\theta)) \\
 &= \frac{3}{2} \left[ \frac{\rho r(\theta)}{f_c} \right]^2 + \frac{m_f}{f_c} \left[ \sigma_m + \frac{\rho r(\theta)}{\sqrt{6}} \right] - 1 \quad (2) \\
 &= 0
 \end{aligned}$$

where  $\sigma_m$ ,  $\rho$  and  $\theta$  denote the coordinates of the Haigh-Westergaard stress space,  $f_c$  the uniaxial compressive strength and the function  $r(\theta)$  describes the variation of the deviatoric strength  $\rho(\theta)$  as a function of the Lode angle in analogy to the elliptic approximation of the five parameter model of Willam and Warnke [16]. While the parameter  $m_f$  is defined as follow:  $m_f = f_c/f_{tt}$ ,  $f_{tt}$  is assumed equal to the uniaxial tensile test as supposed by Rankine criterion. The failure surface showing the meridional sections,  $\theta = 0$  for tensile and  $\theta = \pi/3$  for compressive meridian, are plotted in Fig. 3 at  $\xi = 0.39$  (500°C). As can be observed, the depicted surfaces are smooth and a  $C^1$ -continuous curvilinear trace. Figure 4 shows evolution of the shear strength of the meridian of compression of the envelope as a function of hydrostatic pressure and the degree of dehydration. The surface is smooth and continuous.

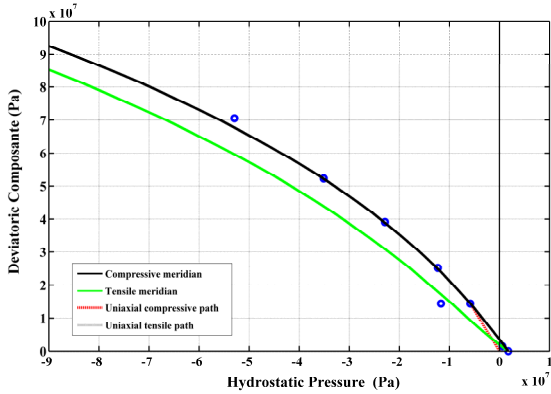


Figure 3: Meridional sections of triaxial failure at  $\xi = 0.39$ (500°C)

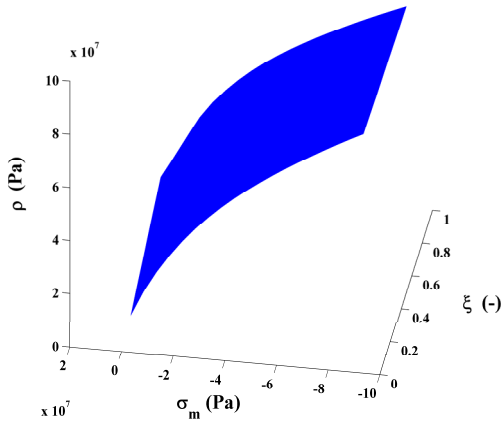


Figure 4: Compressive meridian according to the hydrostatic pressure and the degree of dehydration

As the concrete strength varies with temperature and chemical degradation occurs, appropriate failure envelope can reproduce these changes by expressing the parameters of the model as a function of degree of dehydration  $\xi$ . The failure criterion then becomes:

$$F(\sigma_m, \rho, r(\theta), \xi) = a_f(\xi) \left[ \frac{\rho r(\theta)}{f_c(\xi)} \right]^{\alpha_f(\xi)} + \frac{m_f(\xi)}{f_c(\xi)} \left[ \sigma_m + \frac{\rho r(\theta)}{b_f(\xi)} \right] - 1 = 0 \quad (3)$$

### 3.2 Isotropic hardening and softening loading surfaces

During the hardening stage, the failure surfaces are generated individually by specific values of normalized strength parameter  $k$  where  $0 \leq k \leq 1$ . At the same time, the cohesion parameter  $c$  related to the softening regime remains constant. At the beginning of loading, the elastic regime is limited by a surface loading with initial  $k = k_0$ . The function of the failure envelope as defined in Eq.3 is then modified as follow:

$$F(\sigma_m, \rho, r, k, c, \xi) = \left\{ (1 - k) \left[ \frac{\sigma_m}{f_c(\xi)} + \frac{\rho r(\theta)}{b_f(\xi) f_c(\xi)} \right]^2 + a(\xi) \frac{1}{f_c(\xi)} \left[ \frac{\rho r(\theta)}{f_c(\xi)} \right]^{\alpha_f(\xi)} + \frac{k \beta_f(\xi) m_f(\xi)}{f_c(\xi)} \left[ \sigma_m + \frac{\rho r(\theta)}{b_f(\xi)} \right] - k \beta_f(\xi) c \right\} = 0 \quad (4)$$

The equation 4 serves to define the surface loading and is highly important component of the chemoplastic model. The originality of the proposed triaxial failure function consists in reproducing the hardening of the material both in tension and compression on a wide range of dehydration process. Regardless of the temperature level, this equation was applied at ambient temperature by Hammoud et al [17],

and gave excellent results.

In order to obtain a continuous model taking into account the degradation of strength in a rational manner, the chemoplastic softening model is based on the concept of fracture energy to assess the strength degradation in both tension and compression. For decreasing values of the cohesion parameter  $c$  to zero, the values of tensile strength also tend to zero. At this stage, the remaining resistance may be due to friction between aggregates and binder. The surface failure at the softening varies depending on the setting of decohesion and is expressed by:

$$\begin{aligned} F_s(\sigma_m, \rho, r(\theta), c, \xi) \\ = a_f(\xi) \left[ \frac{\rho r(\theta)}{f_c} \right]^{\alpha_f(\xi)} \\ + \frac{m_f(\xi)}{f_c(\xi)} \left[ \sigma_m + \frac{\rho r(\theta)}{b_f(\xi)} \right] - c = 0 \end{aligned} \quad (5)$$

#### 4 CHEMOPLASTIC POTENTIAL FUNCTION

The elastic response of the material is defined by the generalized Hooke's law by means of the elasticity tensor  $\mathbf{H}$  and the plastic response is governed by the flow rule:

$$\dot{\epsilon}_p = \dot{\lambda} \frac{\partial Q}{\partial \sigma} = \dot{\lambda} m \quad (6)$$

where  $Q$  denotes the chemoplastic potential, and  $\lambda$  is the plastic multiplier. To reduce excessive dilatation in the low confinement region, a non-associated flow rule is introduced. A new chemoplastic potential is defined by re-using the loading function and replacing the adequate set parameters. The chemoplastic potential function is given by the following formula:

$$\begin{aligned} Q(\sigma_m, \rho, r(\theta), \xi) \\ = a_q(\xi) \left[ \frac{\rho r(\theta)}{f_c(\xi)} \right]^{\alpha_q(\xi)} \\ + \frac{m_f(\xi)}{f_c(\xi)} \left[ \sigma_m + \frac{\rho r(\theta)}{b_q(\xi)} \right] - 1 = 0 \end{aligned} \quad (7)$$

To identify the parameters of the chemoplastic potential, it is necessary to know the normal to the potential at rupture for some cases of loading. The relationship between volumetric and deviatoric component of the normal potential must be the same as that obtained in compression tests regardless of the degree of dehydration.

For the chemoplastic potential, it is possible to use circular deviatoric sections (with  $r = 1$ , and  $r(\theta) = 1$ ) instead of the elliptical sections of the failure envelope. The computing time needed to integrate the constitutive law is shorter, and the observed difference, in terms of stress and strain, is negligible. The equation of the chemoplastic potential in the hardening/softening regimes takes the same form as that of the failure surface:

$$\begin{aligned} Q(\sigma_m, \rho, r, k, c, \xi) \\ = \left\{ (1 - k) \left[ \frac{\sigma_m}{f_c(\xi)} + \frac{\rho r(\theta)}{b_q(\xi) f_c(\xi)} \right]^2 \right. \\ \left. + a(\xi) \frac{1}{\alpha_q(\xi)} \frac{\rho r(\theta)}{f_c(\xi)} \right\}^{\alpha_q(\xi)} \\ + \frac{k^{\beta_q(\xi)} m_f(\xi)}{f_c(\xi)} \left[ \sigma_m + \frac{\rho r(\theta)}{b_q(\xi)} \right] - k^{\beta_q(\xi)} c \\ = 0 \end{aligned} \quad (8)$$

#### 5 HARDENING AND SOFTENING PARAMETERS FUNCTIONS

Hardening and softening of concrete can be simulated by varying the shape and location of the loading surface during plastic flow. The strength parameter  $k$  determines the size of the yield or loading surfaces in the hardening regime before the rupture, and is expressed by quadratic function of the accumulated plastic strain  $\epsilon_p$  and a measure of ductility  $d_h$ . The

ductility is also function of degree of dehydration. The function used for  $k$  is:

$$k(\epsilon_p, d_h, \xi) = k_0 + (1 - k_0) \sqrt{\frac{\epsilon_p}{d_h(\xi)} \left( 2 - \frac{\epsilon_p}{d_h(\xi)} \right)} \quad (9)$$

This function is formulated to reach  $k = 1$  when  $\frac{\epsilon_p}{d_h} = 1$ . The rate of equivalent plastic strain  $\epsilon_p$  is determined by the norm of the plastic strain tensor as herein:

$$\dot{\epsilon}_p = \dot{\lambda} \|m\| \quad (10)$$

The measurement of ductility  $d_h$  is used to consider the influence of confinement on the ability of the material to deform permanently. It defined the maximum equivalent plastic strain when the failure envelope is reached. The failure is obtained when the condition  $\frac{\epsilon_p}{d_h} = 1$  is satisfied. Ductility curve is constructed from the equivalent plastic strain at failure obtained during tensile tests, uniaxial compression, and compression with confinement. Since only the equivalent plastic strain of the uniaxial compression and compression with confinement tests are known, other values must be obtained by calculus. The relationship between the ductility and the pressure is shown in Figure 5. The material deforms very little in traction hence its brittle behavior. Two analytic functions are necessary to reproduce the curve of ductility in order to separate the tensile strains from compression.

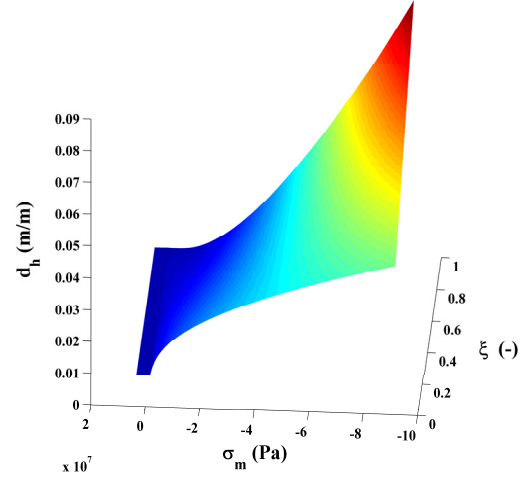


Figure 5: 3D ductility curve versus mean pressure

## 6 STRESS RETURN ALGORITHM

### 6.1 Evaluation of convenient stress for plastic potential

By overlaying the plastic potential on the Etse and Willam yield surface, both defined on the Haigh-Westergaard coordinates, it is possible to observe that, for a given strength parameter  $k$ , the two curves do not undergo through the same stress states. In order to ensure adequate evaluation of normal vectors, it is necessary that each surface goes through the current stress state. Keeping the loading surface unchanged, the calculation related to the plastic potential need to be modified. The solution consisted in identify a new value of deviatoric component  $\rho$  prior to the evaluation of the gradient of plastic potential to move vertically the stress state to the plastic potential for  $Q = 0$ . This method is valid for both hardening and softening. However, it is essential to use circular deviatoric sections and analytical derivatives, to isolate  $\rho$ , then modify the calculation of numerical derivatives. To minimize the potential, the new value of  $\rho$  is obtained using the following iterative relationship:

$$\rho_{i+1} = \rho_i - \frac{Q(\sigma_m, \rho_i, r, k)}{\frac{\partial Q(\sigma_m, \rho_i, r, k)}{\partial \rho}} \quad (11)$$

## 6.2 Resolution scheme

A backward-Euler (Euler implicit) algorithm as defined by Crisfield [18] is applied for constitutive integration. In summary, to calculate the incremental stress  $\Delta\sigma$  from point  $B$  to point  $C$  in Fig. 6, it is necessary to apply the following procedure:

- Calculating the first elastic prediction.

1. From the stress at point  $B$  (Fig.6), calculate the value of  $F$  and the gradient  $n = \frac{\partial F(\sigma_m, \rho, r, k)}{\partial \sigma}$ .

2. In the presence of non-associated flow, identify a particular value of  $\rho$  for  $Q = 0$  and calculated the gradient  $m = \frac{\partial Q(\sigma_m, \rho, r, k)}{\partial \sigma}$ .

3. Compute  $\Delta\lambda = \frac{F_B}{n_B^T H m_B + H_{pB}}$  and the stress at point  $C$ :  $\sigma_C = \sigma_B - \Delta\lambda H m_B$ , where  $\sigma_B$  is the elastic test point,  $H$  is elasticity tensor, and  $H_g$  is effective plastic modulus ( $g$  is generic variable,  $g = p$  for hardening and  $g = c$  for softening).

4. Update the equivalent plastic strain  $\epsilon_p(\epsilon_f)$  in hardening (softening) and the strength parameter  $k(c)$  during the hardening (softening).

- Beginning the implicit backward-Euler method.

5. Calculate  $F$  and  $n$  at the current point  $C$ .

6. Minimize the potential for  $Q = 0$  and calculate the gradient  $m$ .

7. Calculate the residual  $r_0 = \sigma_C - \{\sigma_B - \Delta\lambda H m_C\}$ .

8. Compute the change of the plastic multiplier:

$$\delta\lambda = \frac{F_{C0} - n_C^T \left[ I + \Delta\lambda H \frac{\partial m}{\partial \sigma} \right]_C^{-1} r_0}{n_C^T \left[ I + \Delta\lambda H \frac{\partial m}{\partial \sigma} \right]_C^{-1} H m_C + H_{pC}}$$

change the stresses:

$$\delta\sigma = - \left[ I + \Delta\lambda H \frac{\partial m}{\partial \sigma} \right]_C^{-1} \{r_0 + \delta\lambda H m_C\}$$

9. Update the stress at point  $C$ :  $\sigma_{Cn} = \sigma_{C0} + \delta\sigma$  then calculate the changes in plastic multiplier at point  $B$  (Fig.6):  $\Delta\lambda_n = \Delta\lambda_0 + \delta\lambda$ .

10. Update the equivalent plastic strain  $\epsilon_p(\epsilon_f)$  and the strength parameter  $k(c)$  during the hardening (softening).

11. Repeat the procedure from step 5 until  $r$  and  $F$  are below a certain tolerance.

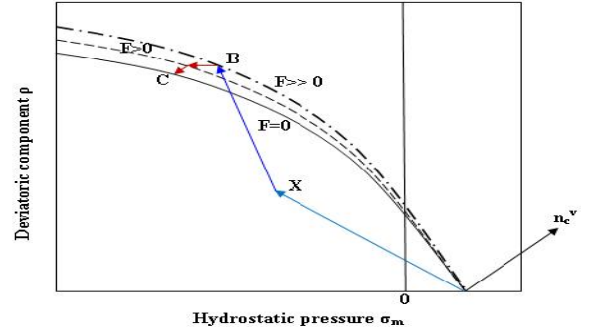


Figure 6: Predictor elastic test point

## 7 MODEL CALIBRATION

Regardless of the temperature levels, calibration procedures were developed in reference [17] and here we summarize some important aspects. The first parameter to identify the failure envelope  $F$  is  $\alpha_f$ . It is used to express the function  $\rho(\sigma_m)$  and its value is set to 2.5. The second parameter is  $\beta_f$  that appears in the hardening term. It is used to define the dependence of the resistance as a function of power of  $k$ . This setting offers the possibility to concrete for hardening in tension, and this loading path is near the triaxial tensile failure. As a first approximation, the parameter  $\beta_f$  is constant and can be similar to the parameter  $\alpha_f$ . These parameters ( $\alpha_f$  and  $\beta_f$ ) are identified manually by trial and error until the criterion provides an accurate fitting of the experimental points. The selected combination is one that offers the lowest error (Root Mean Square) between the measured shear stresses and those defined by the criterion at the same pressures. The same analysis for parameters identification is repeated for the plastic potential. Due to non-associatedness law, the potential has a slightly

different form of the failure envelope. Three parameters ( $a_q, b_q,$  and  $\alpha_q$ ) are need to be identified.

## 8 EVOLUTION OF FAILURE CRITERION AND CHEMOPLASTIC PARAMETERS

### 8.1 Fitting parameters of the failure criterion

Referring to Eq.3 for the failure envelope, the five parameters are expressed as function of the degree of dehydration in order to allow the model to include the strength degradation depending on the degree of dehydration. The first parameter is the absolute value of the uniaxial compressive strength  $f_c$  according to the degree of dehydration  $\xi$  (Fig.1). As the degree of dehydration is directly obtained from the mechanical strength, a linear relationship is obtained between the two variables. The second parameter to fitting is the relationship between the absolute value of the uniaxial compressive strength and the uniaxial tensile strength depending on the degree of dehydration  $\xi$ . As depicted in Fig.7, the relationship is not linear. The last parameters  $a_f$  and  $b_f$  of the loading surface according to the degree of dehydration  $\xi$  are shown in Fig.8. The correlation between the proposed parameters and degree of dehydration offers nonlinear equations. Obviously, a regression using the second order polynomial interpolation is a better representation for these parameters. It was found that the introduction of these new parameters resulted in higher  $R^2$  values. The proposed models can be used to estimate the parameters for intermediate temperature levels and, consequently, determine the failure criteria. Hence, the degree of dehydration helps determine the parameters of the failure envelope. It is therefore possible to plot the shear strength of the compressive meridian of the failure criterion as a function of hydrostatic pressure and the degree of dehydration as shown in Fig 4. The resulting smoothing operation offers convex surface for any stress state. Since this condition is met, this surface makes it possible to determine any stress leading to the rupture

of concrete according to the degree of dehydration.

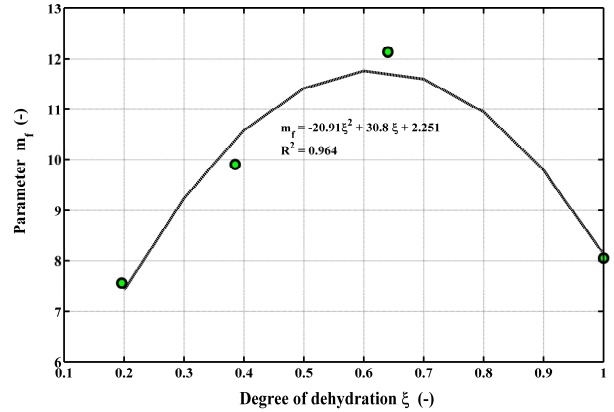
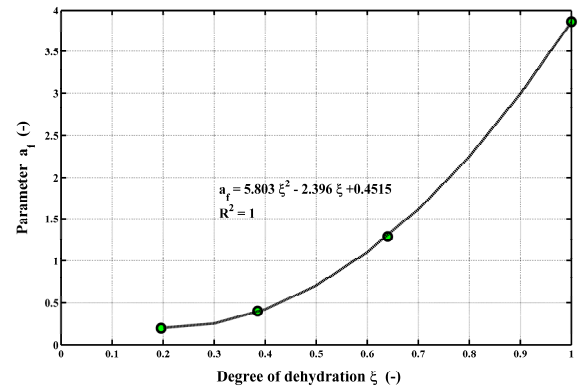
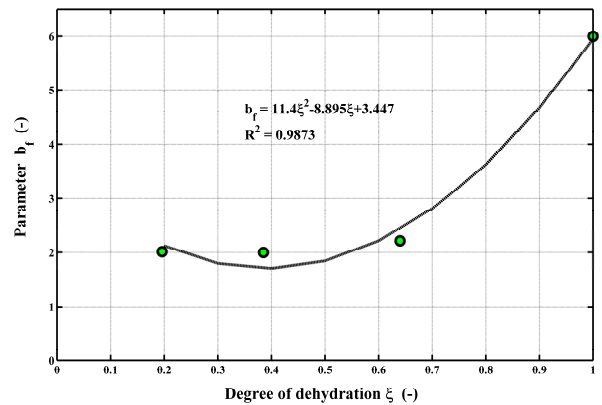


Figure 7: Evolution of  $m_f$  versus degree of dehydration



(a) Parameter  $a_f$

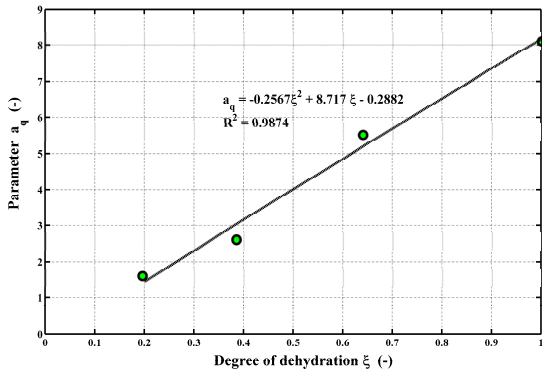


(b) Parameter  $b_f$

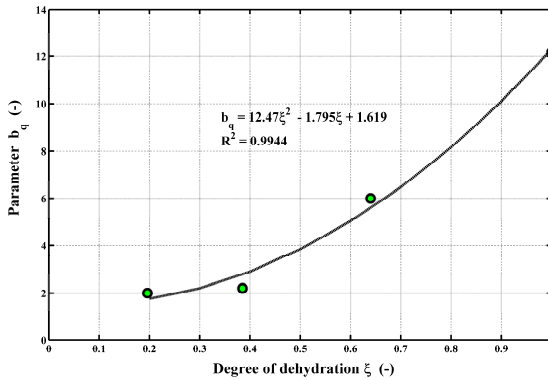
Figure 8: Evolution of failure envelope parameters  $a_f$  and  $b_f$  according the degree of dehydration

### 8.2 Fitting parameters of chemoplastic potential

The first parameters of the chemoplastic potential  $Q$  are  $a_q$  and  $b_q$  different from those of the loading surface. Fig. 9 illustrates the relationship defined as function of the degree of dehydration. Referring to Eq.8, the parameter  $\beta_q$  appears in hardening. It is also different for the failure envelope  $F$  and plastic potential  $Q$  is used to define the dependence of the resistance as a power function. Once all the parameters of potential chemoplastic have been determined, it is now possible to trace this potential across the range of degree of dehydration. As depicted in Fig. 10, the potential obtained is smooth and convex and should not cause numerical problems.



(a) Parameter  $a_q$



(b) Parameter  $b_q$

**Figure 9:** Evolution of failure envelope parameters  $a_q$  and  $b_q$  according the degree of dehydration

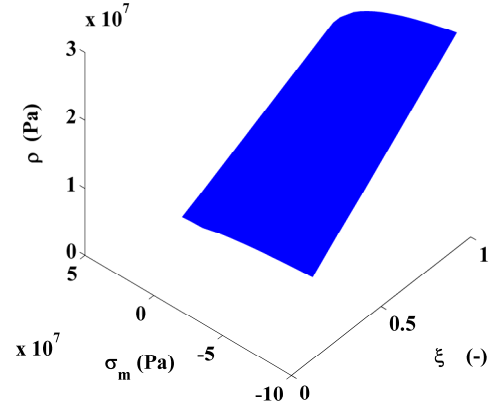


**Figure 10:** Evolution of chemoplastic potential  $Q$  versus degree of dehydration

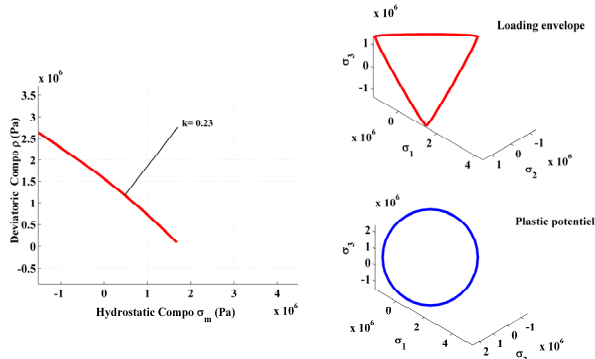
### 9 NUMERICAL EXPERIMENTS FOR VARIOUS LOADING SCENARIOS

The present constitutive model was implemented in Matlab. It has to be noted that all model parameters were calibrated on the basis of the experimental studies from Hammoud et al [19]. The capability and performance of the model is evaluated by comparisons with experimental results. As depicted in Figures 11 and 12, results of simulation of a direct tension at 500°C, the failure criterion is similar to that of Rankine criterion. The model slightly overestimates the resistance calculated analytically for this loading case. Figure 13 shows the stress-strain simulation for the triaxial tension. The failure criterion is also close to that of Rankine. Based on that criterion, the model correctly estimates the strength of the material. Regardless the temperature treatment, the model assumes that the material does not present hardening stage. The main crack propagation is failing its residual strength as if the material behaved fragile.

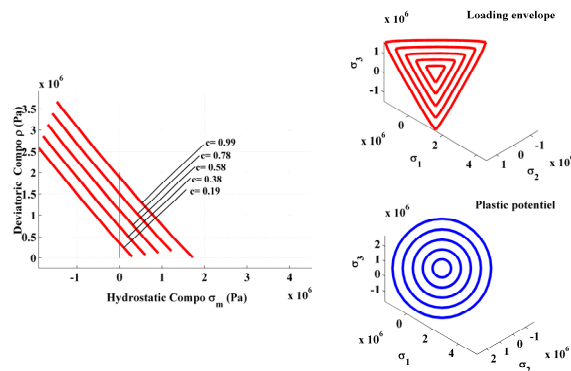
Figures 14 and 15 show comparison between numerical and experimental results for concrete under uniaxial compression at 300°C, in both axial and radial directions. The correlation is reasonable. The hardening regime is similar to that measured experimentally. At this temperature level, the model slightly overestimates the axial stress. As can be observed in Figures 15(a) and 15(b), the failure criterion and the plastic potential go

through the same strength parameter  $k$ (or cohesion  $c$ ) as explained in section 6.1.

Figure 16 shows comparison between numerical and experimental results for concrete under triaxial compression and various confinement levels at 300°C. The correlation is acceptable for both axial and radial directions. The respective experimental data are relatively close to the numerical result.



(a) Hardening



(b) Softening

Figure 11: Numerical uniaxial tension test in hardening and softening stages at  $\xi = 0.39(500^\circ\text{C})$

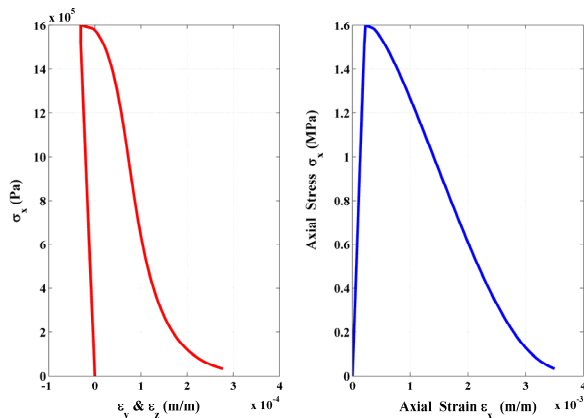


Figure 12: Stress-strains (axial and radial) curves from numerical uniaxial tension test at  $\xi = 0.39(500^\circ\text{C})$

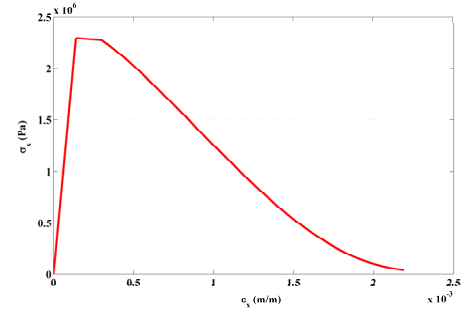


Figure 13: Stress-strain curve from numerical triaxial tension test at  $\xi = 0.64(300^\circ\text{C})$

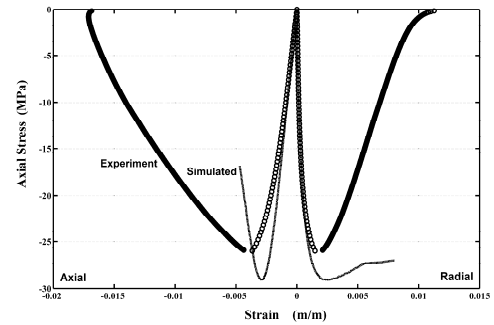
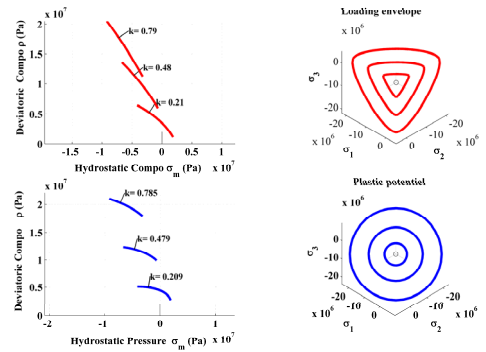
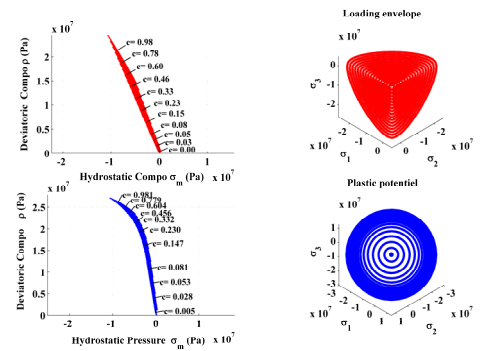


Figure 14: Stress-strain curves in axial compression at  $\xi = 0.64(300^\circ\text{C})$



(a) Hardening



(b) Softening

Figure 15: Hardening and softening stages in axial compression test at  $\xi=0.64(300^\circ\text{C})$

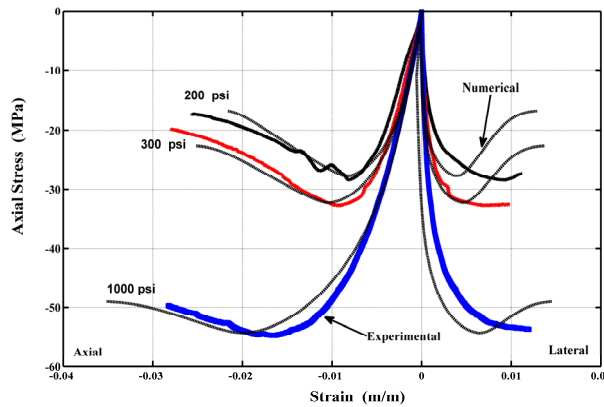


**Figure 16:** Comparison between numerical and experimental results for concrete under triaxial compression at different confinement pressures at  $\xi=0.64(300^{\circ}\text{C})$

## 10 CONCLUSIONS

Novel tri-dimensional constitutive model was proposed and investigated. Simulations were performed to assist in the development of the modeling requirements for simulating high temperature impact on concrete material. A three dimensional constitutive law, based on the *ELM* model, under chemoplastic framework has been formulated. The core of proposed model was composed of: (1) an expanded a five parameter loading surface under chemoplastic framework to consider chemoplastic softening and, consequently, the decrease of the strength domain of concrete at high temperature. The loading surface was calibrated against database of test results. (2) A new ductility function was proposed and calibrated through the experimental results. This operation was performed to better capture the evolution of the plastic deformation under elevations of both temperature and confinement pressure. (3) New chemoplastic potential was also proposed and calibrated via experimental results.

Simulation results have been compared to experimental data in terms of stress-strains relationships. Analyses have shown that simulation results using this new formulation were close to experimental data and in good agreement compared with available numerical experimental results on the wide range of temperature levels.

## Acknowledgements

The author acknowledges the financial support from the Fonds de recherche du Québec- Nature et technologies (FRQNT).

## REFERENCES

- [1] Phan, M., Meftah, F., Rigobert, S., Autori, P., Lenglet, C., Dal Pont, S., 2011. A finite element modeling of thermo-hydro-mechanical behavior and numerical simulations of progressing spalling front. *Procedia Engineering*. **10**:3128-3133.
- [2] Phan, L., Lawson, J., Davis, F., 2001. Effects of elevated temperature exposure on heating characteristics, spalling, and residual properties of high performance concrete. *Materials and Structures*. **34**:83-91.
- [3] Pihlajavaara, S., 1972. An analysis of the factors exerting effect on strength and other properties of concrete at high temperature. *American Concrete Institute; Special Publication SP-34*, Farmington Hills, 1972, USA.
- [4] Ahmade, S., Hamoush, S., 1988. A constitutive model for concrete exposed to high temperature. In *Elastic plastic failure modeling of structures with applications. ASME Pressure Vessels and Piping conference*; New York, NY, USA; pp: 145-152
- [5] Khennane, A., Baker, G., 1992. Plasticity models for biaxial behavior of concrete at elevated temperature. Part I: Failure criterion. *Computer Methods in Applied Mechanics and Engineering*. **100**: 207-223.
- [6] Nechnech, W., Meftah, F., Reynouard, J., 2002. An elasto-plastic damage model for plain concrete subjected to high temperatures. *Engineering and Structures*. **24**:597-611.

- [7] Luccioni, B., Figueora, M., Danesi, R., 2003. Thermo-mechanic model for concrete exposed to elevated temperatures. *Engineering and Structures*. **25**: 729-742.
- [8] Yang, B., Dafalias, Y., Herrmann, L., 1985. A bounding surface plasticity model for concrete. *International Journal of Engineering Mechanics*. **111**: 359-380.
- [9] Ulm, F., Coussy, O., Bazant, Z., 1999. The "Chunnel" fire. I: Chemoplastic softening in rapidly heated concrete. *Journal of Engineering Mechanics*. **125**: 272-282.
- [10] Ulm, F., Coussy, O., 1995. Modeling of thermo-chemo-mechanical couplings of concrete at early age. *Journal of Engineering Mechanics*. **121**: 785-794.
- [11] Ulm, F., Coussy, O., 1996. Strength growth as chemo-plastic hardening in early age concrete. *Journal of Engineering Mechanics*. **122**: 1123-1132.
- [12] Coussy, O., 1995. *Mechanics of porous media*. John Wiley & Sons Ltd. Chichester, UK.
- [13] Cervera, M., Oliver, J., Prato, T., 1999. Thermo-chemo-mechanical model for concrete. I: Hydration and aging. *Journal of Engineering Mechanics*. **125**: 1018-1027.
- [14] Hellmich, C., Ulm, F.J., Mang, H., 1999. Multisurface chemoplasticity. I: Material for shotcrete. *Journal of Engineering Mechanics*. **125**:692-701.
- [15] Etse, G., Willam, K., 1994. Fracture energy formulation for inelastic behavior of plain concrete. *Journal of Engineering Mechanics*. **120**:1983-2011.
- [16] Willam, K., Wranke, E., 1975. Constitutive Model for triaxial behavior of concrete. In: *Concrete Structure Subjected to Triaxial Stresses*. International Association for Bridge and Structural Engineering, Zurich, Suisse. pp: 1-30.
- [17] Hammoud, R., Boukhili, R., Ammar, Y., 2012. Unified formulation for a triaxial elastoplastic constitutive law for concrete. (in preparation).
- [18] Crisfield, M., 1991. *Non-linear finite element analysis of solids and structures*. John Wiley & Sons, England.
- [19] Hammoud, R., Yahia, A., Boukhili, R., 2012. Triaxial residual stress-strain behavior of concrete after being subjected to high temperature. (in preparation).